

See discussions, stats, and author profiles for this publication at: <https://www.researchgate.net/publication/284209480>

Small Molecules Based on Alkyl/Alkylthio-thieno[3,2-b]thiophene-Substituted Benzo[1,2-b:4,5-b']dithiophene for Solution-Processed Solar Cells with High Performance

ARTICLE *in* CHEMISTRY OF MATERIALS · NOVEMBER 2015

Impact Factor: 8.35 · DOI: 10.1021/acs.chemmater.5b03889

READS

73

11 AUTHORS, INCLUDING:



Bin Kan

Nankai University

31 PUBLICATIONS 659 CITATIONS

[SEE PROFILE](#)



Xuan Yang

Nankai University

16 PUBLICATIONS 198 CITATIONS

[SEE PROFILE](#)



Mingtao Zhang

Nankai University

27 PUBLICATIONS 467 CITATIONS

[SEE PROFILE](#)



Yongsheng Chen

Georgia Institute of Technology

314 PUBLICATIONS 17,735 CITATIONS

[SEE PROFILE](#)

Small Molecules Based on Alkyl/Alkylthio-thieno[3,2-*b*]thiophene-Substituted Benzo[1,2-*b*:4,5-*b*']dithiophene for Solution-Processed Solar Cells with High Performance

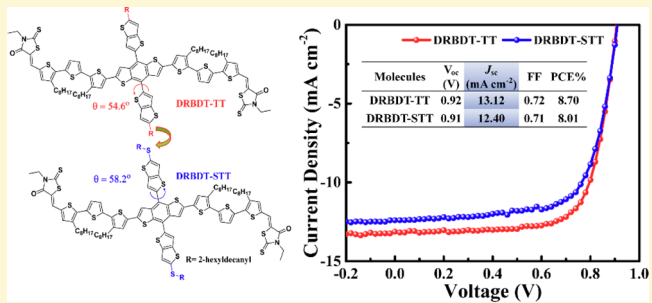
Bin Kan,^{†,‡,||} Qian Zhang,^{†,‡,||} Feng Liu,[§] Xiangjian Wan,^{*,†,‡} Yunchuang Wang,^{†,‡} Wang Ni,^{†,‡} Xuan Yang,^{†,‡} Mingtao Zhang,^{†,‡} Hongtao Zhang,^{†,‡} Thomas P. Russell,[§] and Yongsheng Chen^{*,†,‡}

[†]State Key Laboratory and Institute of Elemento-Organic Chemistry, Collaborative Innovation Center of Chemical Science and Engineering (Tianjin), School of Materials Science and Engineering, and [‡]Key Laboratory of Functional Polymer Materials and the Centre of Nanoscale Science and Technology, Institute of Polymer Chemistry, College of Chemistry, Nankai University, Tianjin 300071, China

[§]Polymer Science and Engineering Department, University of Massachusetts, Amherst, Massachusetts 01003, United States

S Supporting Information

ABSTRACT: Two acceptor-donor-acceptor small molecules based on thieno[3,2-*b*]-thiophene-substituted benzo[1,2-*b*:4,5-*b'*]dithiophene, DRBDT-TT with alkyl side chain and DRBDT-STT with alkylthio side chain, were designed and synthesized. Both molecules exhibit good thermal stability, suitable energy levels, and ordered molecular packing. Replacing the alkyl chain with alkylthio increases the dihedral angle between the thieno[3,2-*b*]thiophene (TT) and benzo[1,2-*b*:4,5-*b'*]dithiophene (BDT) unit, and thus slightly decreases its intermolecular interactions leading to its blue-shift absorption in the solid state. The best devices based on DRBDT-TT and DRBDT-STT both exhibited power conversion 0.70 under AM 1.5G irradiation (100 mW cm⁻²), which are attr 30 nm and well-balanced charge transport properties. The device current density (J_{sc}) and thus slightly lower PCE as compared to absorption. These results demonstrate that thieno[3,2-*b*]thiophene be promising donor materials for obtaining high efficiencies an



■ INTRODUCTION

Organic photovoltaics (OPVs) with bulk heterojunction (BHJ) architectures have been considered a promising solar energy conversion technology possessing the advantages of solution-processability, lightweight, low-cost, and flexibility.^{1,2} As compared to the widely investigated polymer-based OPVs (P-OPVs),^{3–8} small/oligomer-molecule-based OPVs (SM-OPVs) have made a great stride with encouraging power conversion efficiencies (PCEs) over 10%,^{9–11} which is comparable to the best performance of P-OPVs.^{12–17} This progress is attributed to the development of photoactive materials, along with innovations and optimizations in device processing.^{18–26} Besides, understanding the structure–property relationships for the further optimization of OPVs has become an important topic in the field of soft matter and will provide theoretical basis for new molecular material design. In the view of the advantages of small molecules, including well-defined but versatile chemical structures, thus easier energy level control, mobility tuning, and no batch-to-batch variations, small molecules are believed to be candidates not only for providing more reliable analyses of chemical structure–properties–device

performance relationships but also for achieving higher OPV performance.^{23,27–30}

Photoactive material innovation, including donor and acceptor materials, is one of the major forces currently driving the performance for both polymer and small molecule-based OPVs forward.^{20,31–38} Considering various molecules designed for solution processed solar cells with high OPV performance, benzo[1,2-b:4,5-b']dithiophene (BDT) is a promising building block for both polymers and small molecules due to its symmetric and planar conjugated structure.^{39–42} Thieno[3,2-b]thiophene (TT) unit is of particular interest in the synthesis of low bandgap polymers for high-performance organic field-effect transistors and P-OPVs due to its stable quinoidal structure.^{43,44} Lately, Hwang et al. reported that the introduction of TT onto the BDT unit provided efficient π -orbital overlap between conjugated polymer chains, enhanced molecular ordering, and hole mobility, which are beneficial for

Received: October 3, 2015

Revised: November 12, 2015

getting high fill factors (FFs).^{45,46} These results imply that TT-substituted BDT unit would be a promising building unit for high performance donor materials. In addition, alkylthio side chain has been widely employed in organic semiconductors, which usually exhibits better performance than its alkyl-substituted analogue molecules.^{10,47–50} Recently, the influence of changing the side chain from alkyl to alkylthio on their properties for TT-substituted BDT-based polymers has been well studied, and the polymer material based on alkylthio-TT-substituted BDT (PSTTBBDT-FTT) exhibits better performance than the polymer based on alkyl-TT-substituted BDT (PTTBBDT-FTT), which is attributed to its more red-shifted absorption spectra and higher hole mobility.⁵¹ So far, the OPV performance of TT-substituted BDT-based small molecules and whether its alkylthio derivative still possesses better performance than its alkyl derivative have not been investigated.

Herein, we designed and synthesized two new acceptor-donor-acceptor (A–D–A) type small molecules, DRBDT-TT with alkyl-TT-substituted BDT as the central building block, and DRBDT-STT with alkylthio-TT-substituted BDT as the central building block, respectively. 3-Ethylrhodanine was selected as the ending groups, and their specific chemical structures are depicted in Figure 1. The photovoltaic

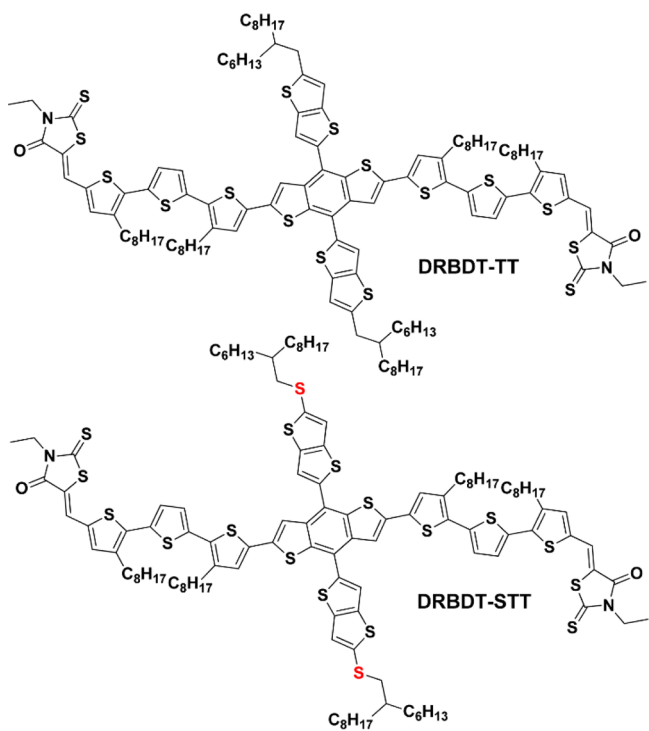


Figure 1. Chemical structures of the target molecules DRBDT-TT and DRBDT-STT.

performance based on these two molecules was systematically investigated, and high efficiencies over 8% with high FFs over 0.70 were obtained for the devices based on these two small molecules. Nevertheless, the devices based on DRBDT-STT with alkylthio side chains exhibited a PCE of 8.01%, slightly lower than 8.70% for DRBDT-TT due to its relatively poorer absorption, which is surprisingly contrary to the observed performances of their corresponding counterparts for P-OPVs. These results demonstrated that while TT-substituted BDT derivatives could be promising donor materials for SM-OPVs, further studies for the structure–performance are highly

needed for the complicated engineering of small-molecule donor materials for high performance.

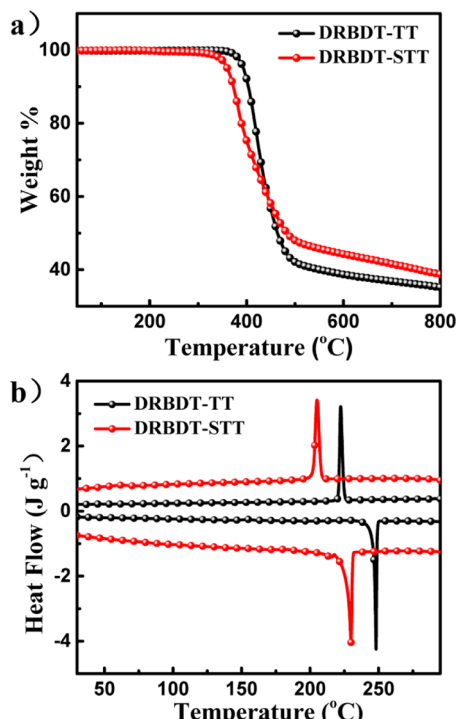
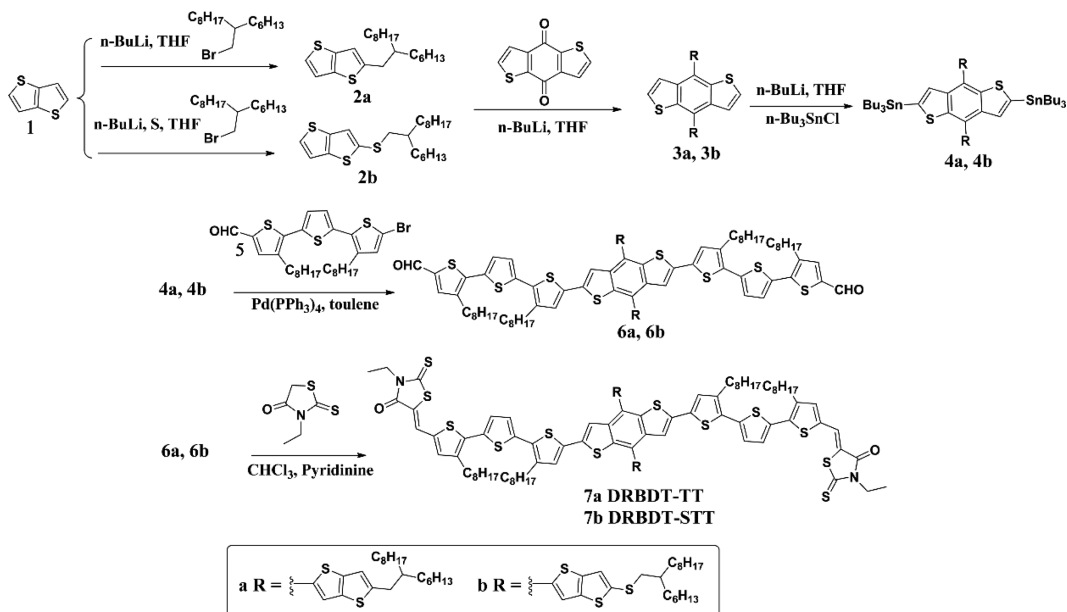
RESULTS AND DISCUSSION

Material Synthesis. The detailed synthetic procedures and characterization data for DRBDT-TT and DRBDT-STT are presented in the Experimental Section (Scheme 1). The intermediates of dialdehyde compounds **6a** and **6b** were synthesized through Stille coupling between compounds **4a** or **4b** and **5**, respectively. The target molecules were then prepared by Knoevenagel condensation of the dialdehyde compounds with 3-ethylrhodanine. Purification using conventional chromatography with silica gel and then recrystallization from chloroform and hexane offered the final products, and the purity was verified by NMR, elemental analysis, and time-of-flight (MALDI-TOF) MS. These two molecules exhibit good solubility in common organic solvents, such as chloroform, chlorobenzene, etc.

Thermal Stability. Thermogravimetric analysis (TGA) (Figure 2a) suggests that both molecules possess a decomposition temperature (T_d) over 350 °C under N₂ atmosphere, which indicates that the thermal stability of these molecules is adequate for application in OPVs. Differential scanning calorimetry (DSC) analysis for both molecules, shown in Figure 2b, exhibits clear melting temperatures (T_m) on the heating process and recrystallization points (T_c) on the cooling process, indicating that DRBDT-TT and DRBDT-STT have a tendency to crystallize. In comparison with DRBDT-TT, DRBDT-STT shows a decrease in both T_m and T_c of nearly 20 °C, together with an obvious decrease in their enthalpies (ΔH_m and ΔH_c) associated with each process, implying that the introduction of alkylthio side chain weakened the molecular thermal robustness and intermolecular interactions. The detailed data are listed in Table 1.

Optical Absorption and Electrochemical Properties. The UV–vis absorption spectra of DRBDT-TT and DRBDT-STT in diluted CHCl₃ solution and in solid film are shown in Figure 3a, and the corresponding data are summarized in Table 2. The absorption of DRBDT-TT solution shows a maximum absorption peak (λ_{\max}) at 509 nm and a high maximum absorption coefficient of $1.07 \times 10^5 \text{ M}^{-1} \text{ cm}^{-1}$. After introducing the alkylthio chain, DRBDT-STT in solution shows a slight blue-shift of 2 nm at λ_{\max} and the same maximum absorption coefficient in comparison with DRBDT-TT. In the solid state, these two molecules display similar absorption patterns with an obvious red-shifted and broadened absorption as compared to their solutions. In addition, distinct shoulder peaks at 635 and 631 nm are observed for DRBDT-TT and DRBDT-STT, respectively, indicative of an effective molecular packing between molecular backbones, which is beneficial for charge transport. Overall, DRBDT-STT shows a slight blue-shift in the film state as compared to DRBDT-TT, which may be attributed to its larger dihedral angle between alkylthio-TT and BDT unit than that between alkyl-TT and BDT unit (Figure S1), and hence its slightly weaker molecular packing as evidenced by DSC and GIXD results. The optical band gaps, estimated from the onset of the film absorption, are 1.78 and 1.80 eV for DRBDT-TT and DRBDT-STT, respectively.

Cyclic voltammetry (CV) was used to investigate the molecules' energy levels. As shown in Figure 3c, the HOMO and LUMO energy levels, calculated from the onset oxidation and reduction potential, are −5.13 and −3.33 eV for DRBDT-TT, and −5.15 and −3.34 eV for DRBDT-STT, respectively.

Scheme 1. Synthetic Procedures of DRBDT-TT and DRBDT-STT**Figure 2.** (a) TGA plot of DRBDT-TT and DRBDT-STT; and (b) DSC plot of DRBDT-TT and DRBDT-STT.**Table 1.** Thermal Property Data of DRBDT-TT and DRBDT-STT

molecules	T_d (°C)	T_m (°C)	ΔH_m (J g ⁻¹)	T_{cr} (°C)	ΔH_c (J g ⁻¹)
DRBDT-TT	393	248	-38.34	222	30.70
DRBDT-STT	360	230	-30.80	205	19.72

The electrochemical band gaps of DRBDT-TT and DRBDT-STT are estimated to be 1.80 and 1.81 eV, which are consistent with their optical band gaps. These data suggest that DRBDT-

TT and DRBDT-STT would be promising donor materials for SM-OPVs.

Photovoltaic Performance. Solution-processed BHJ devices were fabricated using DRBDT-TT and DRBDT-STT as the electron donor with a conventional device structure of ITO/PEDOT:PSS/donor:PC₇₁BM/PFN-Br/Al (where PFN-Br is poly[(9,9-bis(3'-(*N,N*-dimethyl)-*N*-ethylammonium)-propyl]-2,7-fluorene)-*alt*-2,7-(9,9-dioctylfluorene)]-dibromide).⁵² The optimized blend ratio for these two donor materials was 1:0.8 (donor:PC₇₁BM) by weight. Recently, our and many other groups have demonstrated that solvent vapor annealing (SVA) treatment can fine-tune the morphology of the active layers and hence enhance the performance of SM-OPVs.^{24,25,53–55} Thus, we used SVA in the device optimization process. The *J*–*V* curves of the devices without treatment and with SVA were presented in Figure 4, and the corresponding photovoltaic parameters are summarized in Table 3. The devices based on DRBDT-TT and DRBDT-STT without SVA yielded moderate PCEs of 6.85% and 5.56%, respectively, with low short-circuit current densities (*J*_{sc}) and FFs. After SVA treatment, the performances of the devices based on these two donor materials were enhanced as a result of significant enhancement of *J*_{sc} and FF (Table 3). Particularly, the OPV devices based on these two molecules both obtained PCEs over 8%, with high open-circuit voltages (*V*_{oc}) over 0.90 V and remarkable FFs over 0.70. The optimized devices based on DRBDT-TT exhibited a PCE of 8.70% with a *V*_{oc} of 0.92 V, a *J*_{sc} of 13.12 mA cm⁻², and an outstanding FF of 0.72. The devices based on DRBDT-STT exhibited a PCE of 8.01%, relatively lower than for the DRBDT-TT, mainly due to its lower *J*_{sc} (Table 3), which might have originated from its relatively poorer absorption. It should be pointed out that both optimized devices exhibited similar high FFs (over 0.70), implying that any difference in charge recombination loss in the devices could be neglected,^{56–59} which can be evidenced by the morphology and mobility analysis as discussed below.

To investigate the reason for the different device performance between DRBDT-TT and DRBDT-STT, UV-vis absorption spectra of their blend films and the external

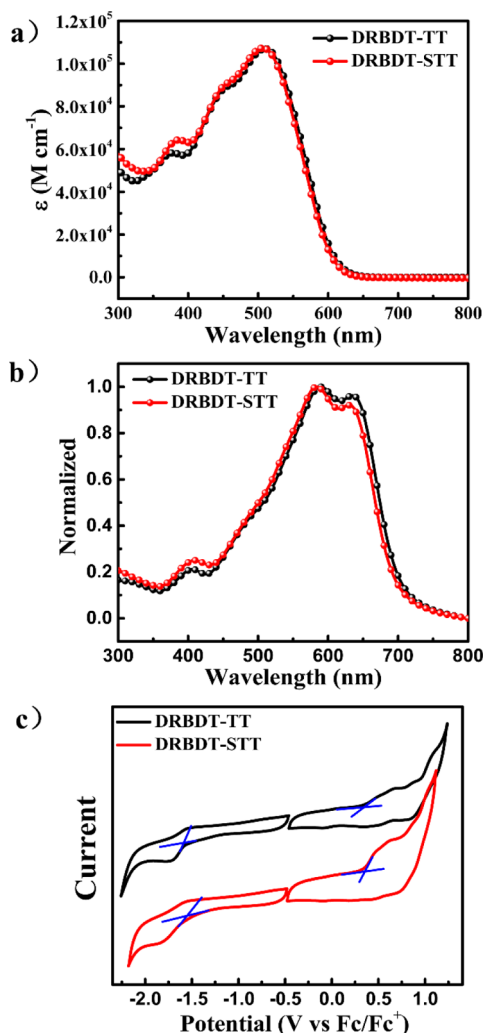


Figure 3. (a) UV–vis absorption spectra of DRBDT-TT and DRBDT-STT solutions; (b) UV–vis absorption spectra of DRBDT-TT and DRBDT-STT films; and (c) cyclic voltammograms of DRBDT-TT and DRBDT-STT in dichloromethane solutions.

quantum efficiency (EQE) with SVA treatment were measured. Figure 5a shows the absorption spectra of DRBDT-TT:PC₇₁BM and DRBDT-STT:PC₇₁BM films under their optimized conditions. Obvious shoulder peaks at \sim 631 nm appeared for both films, which are related to the ordered molecular packing. It is worth noting that the absorption intensity for the DRBDT-STT:PC₇₁BM film is obviously lower than that for the DRBDT-TT:PC₇₁BM film, thus leading to a relatively lower J_{sc} . EQEs of the best devices are shown in Figure 5b, where the devices with DRBDT-TT and DRBDT-STT exhibit photo-current responses from 300 to 800 nm with a maximum value of 73% and 70%, respectively. In addition, EQEs over 65% across the range of 420–600 nm are observed, indicating that the photoelectron conversion process is efficient for both optimized devices. In general, the EQE for

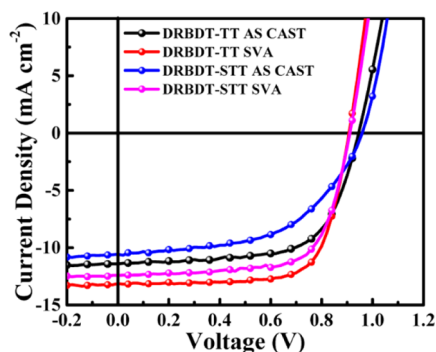


Figure 4. Current density–voltage (J – V) characteristics of both devices without treatment and with SVA treatment.

the DRBDT-STT-based devices is lower than that for the DRBDT-TT-based devices. These results are consistent with the trend of the above UV–vis absorption results. The calculated J_{sc} 's obtained by integration of the EQE curves are listed in Table 3, which show a 3–5% mismatch as compared to the J_{sc} values obtained from their J – V curves.

Morphology and Mobility. The optimized active layer morphologies were measured by atomic force microscopy (AFM) and transmission electron microscopy (TEM). From AFM images (Figure 6a and b), it can be seen that the surfaces of DRBDT-TT:PC₇₁BM and DRBDT-STT:PC₇₁BM films are uniform and smooth with root-mean-square (rms) surface roughness values of 1.21 and 1.48 nm, respectively. Coarse domain features of about 20–30 nm and well-interpenetrating networks with obvious phase separation are formed for both optimized blend films. From the TEM images (Figure 6c and d), defined phased separations of the donor and acceptor were observed in both blend films, and well-developed nanofibrillar structures with a bicontinuous interpenetrating network could also be observed. All of these may be beneficial for exciton dissociation and charge transport, and thus getting high FFs.⁶⁰ Resonant soft X-ray scattering (RSoSXS) (Figure 6e and Table 4) on the DRBDT-TT:PC₇₁BM blend shows an interference ($q = 0.0123 \text{ \AA}^{-1}$) corresponding to a domain center-to-center distance of 51 nm. RSoSXS for the DRBDT-STT:PC₇₁BM blend exhibits an interference at $q = 0.0104 \text{ \AA}^{-1}$, corresponding to a center-to-center distance of 60 nm.

The microstructures of the optimized pure and blend films were further characterized by two-dimensional grazing incidence X-ray diffraction (2D-GIXD). Out-of-plane and in-plane line cuts of GIXD of blend films are presented in Figure 7. As shown in Figure 7a–d, multiple higher order ($h00$) reflections for pure films and blend films along the q_z direction are observed for both DRBDT-TT and DRBDT-STT, indicative of a long-range order and crystallinity both in their pure and blend films.⁶¹ For the pure films, DRBDT-TT and DRBDT-STT show a (010) reflection, characteristic of π – π stacking, along the q_{xy} direction, that is, in the plane of the film, indicating that both molecules have a preferred edge-on orientation relative to the substrate. (010) peaks for DRBDT-

Table 2. Optical and Electrochemical Data of DRBDT-TT and DRBDT-STT

molecules	UV–vis				CV		
	$\lambda_{\max,\text{sol}}$ (nm)	ϵ ($M\text{ cm}^{-1}$)	$\lambda_{\max,\text{film}}$ (nm)	E_g^{opt} (eV)	HOMO (eV)	LUMO (eV)	E_g^{CV} (eV)
DRBDT-TT	509	1.07×10^5	589, 635	1.78	-5.13	-3.33	1.80
DRBDT-STT	507	1.07×10^5	584, 631	1.80	-5.15	-3.34	1.81

Table 3. Average Photovoltaic Performance of DRBDT-TT and DRBDT-STT-Based Devices^a

molecules	treatment	V_{oc} (V)	J_{sc} (mA cm ⁻²)	FF	PCE %	J_{sc}^{cal} (mA cm ⁻²)
DRBDT-TT	as-cast	0.93 ± 0.01 (0.94)	11.20 ± 0.15 (11.40)	0.63 ± 0.01 (0.64)	6.67 ± 0.14 (6.85)	11.21
	SVA	0.91 ± 0.01 (0.92)	12.93 ± 0.17 (13.12)	0.71 ± 0.01 (0.72)	8.50 ± 0.17 (8.70)	12.50
DRBDT-STT	as-cast	0.95 ± 0.01 (0.96)	10.45 ± 0.27 (10.75)	0.53 ± 0.01 (0.54)	5.34 ± 0.20 (5.57)	10.19
	SVA	0.90 ± 0.01 (0.91)	12.20 ± 0.14 (12.40)	0.70 ± 0.01 (0.71)	7.85 ± 0.13 (8.01)	11.97

^aThe best results are provided in parentheses.

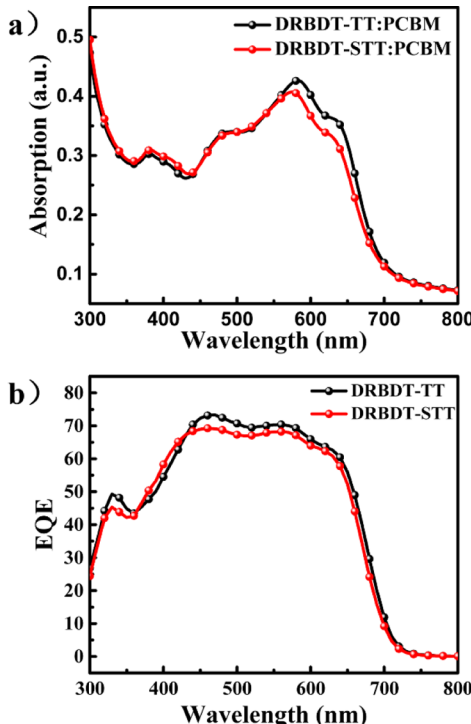


Figure 5. (a) The absorption spectra of DRBDT-TT:PC₇₁BM and DRBDT-STT:PC₇₁BM films with SVA treatment; and (b) the EQE curves of DRBDT-TT and DRBDT-STT-based devices with SVA treatment.

TT and DRBDT-STT were located at 1.72 and 1.69 Å⁻¹, giving a π–π stacking distance of 3.66 and 3.72 Å, respectively. The (100) peaks along the q_z direction of DRBDT-TT and DRBDT-STT are both observed at 0.273 Å⁻¹, corresponding to their alkyl-to-alkyl distance of 23.0 Å.

For their optimized blend films, the GIXD patterns with obvious (h00) reflections are similar to those observed in the pure films, and the corresponding (100) and (010) distances in the blend films are summarized in Table 4. In comparison with their pure films, there is little change in their alkyl-to-alkyl distance and π–π stacking distance by the presence of blended PC₇₁BM molecules. The DRBDT-TT and DRBDT-STT still adopt a preferred edge-on orientation in blend films. It should be noted that DRBDT-STT exhibits a slightly larger π–π stacking distance than DRBDT-TT both in pure and in blend films, which reveals that replacing the alkyl (for DRBDT-TT) with the alkylthio (for DRBDT-STT) indeed slightly weakens its intermolecular interactions as discussed above. The crystal size is estimated using Scherrer analysis⁶² to be 141 and 150 Å for DRBDT-TT:PC₇₁BM and DRBDT-STT:PC₇₁BM along the direction of (100), respectively. These results, in combination with the morphological results measured by AFM, TEM, and RSoXS, indicate effective exciton diffusion/dissociation and charge transport processes occurred in the DRBDT-

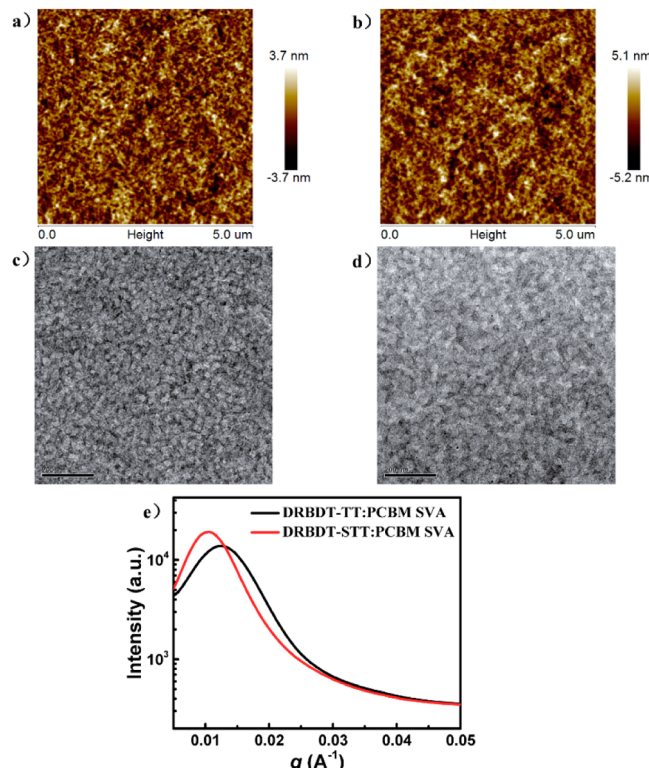


Figure 6. Tapping-mode AFM height images of (a) DRBDT-TT:PC₇₁BM blend films and (b) DRBDT-STT:PC₇₁BM blend films, and TEM images of (c) DRBDT-TT:PC₇₁BM blend films and (d) DRBDT-STT:PC₇₁BM blend films with SVA treatment. The scale bars are 200 nm. (e) RSoXS profiles of DRBDT-TT:PC₇₁BM and DRBDT-STT:PC₇₁BM blend films with SVA treatment.

TT:PC₇₁BM and DRBDT-STT:PC₇₁BM optimized devices, thus leading to their high FFs.^{57,60}

The mobilities of the optimized devices were measured by the space charge limited current (SCLC) method (Figure S2). The hole and electron mobilities for DRBDT-TT-based best devices are 5.41×10^{-4} and 5.27×10^{-4} cm² V⁻¹ s⁻¹, respectively. For DRBDT-STT-based best devices, the hole and electron mobilities are 4.74×10^{-4} and 5.05×10^{-4} cm² V⁻¹ s⁻¹, respectively, which are slightly lower than those for DRBDT-TT-based devices because of its larger π–π stacking distance. The charge carrier ratios between electron and hole are close to unity for both optimized devices based on DRBDT-TT and DRBDT-STT, indicative of a well-balanced charge transport ability, and thus leading to their high FFs.⁵⁶ These results are well consistent with their morphological results as discussed above.

Generally, the introduction of alkylthio chain on the aromatic unit for polymers and small molecules could result in more ordered molecular packing in contrast to their analogue molecules. For examples, polymer PBDTTT-S-TT⁵⁰ and

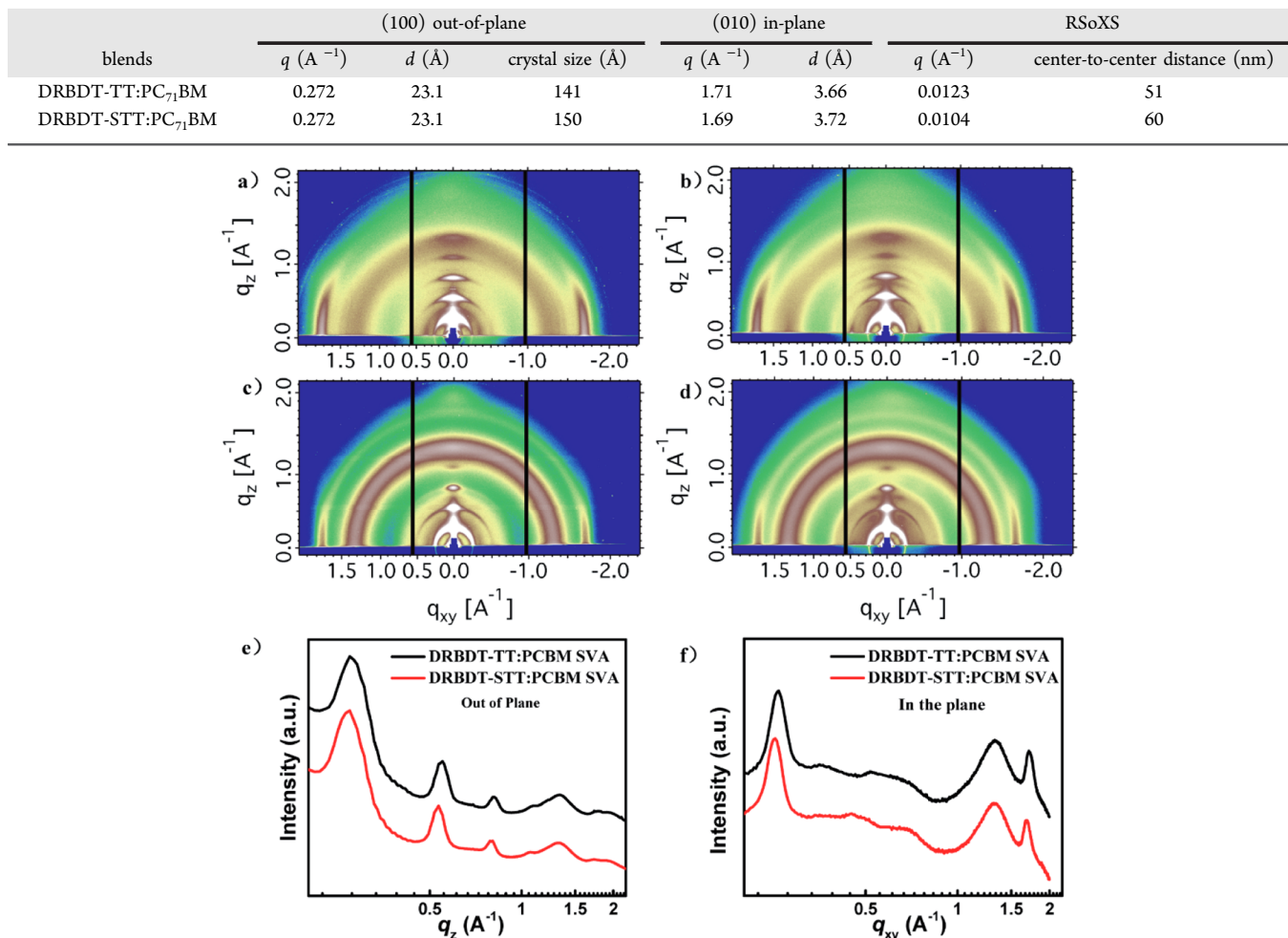
Table 4. Morphological Data of GIXD and RSoXS

Figure 7. GIXD patterns for pure films (a) DRBDT-TT, (b) DRBDT-STT, and blend films of (c) DRBDT-TT:PC₇₁BM and (d) DRBDT-STT:PC₇₁BM. (e) Out-of-plane line cuts and (f) in-plane line cuts of the GIXD patterns for the blend films. The films were prepared under the optimized conditions.

small molecule DR3TSBDT¹⁰ all showed better packing behavior and gave higher device performances as compared to their counterpart polymer and small molecule. However, herein, it gave an opposite result. In fact, if we study the small molecular structures further, such results might not be so surprising at all. The optimized geometries for DRBDT-TT and DRBDT-STT, based on the density functional theory (DFT) calculations, are presented in Figure S1. It can be seen that both molecules exhibit a linear backbone conformation from the side view, which means that DRBDT-TT and DRBDT-STT have good coplanarity. Yet, the dihedral angle between alkylthio-TT and BDT unit is 58.2° for DRBDT-STT, slightly larger than 54.6° for DRBDT-TT. Thus, this difference might result in different UV-vis absorption and $\pi-\pi$ stacking distances as evidenced above, and thus their different OPV performance. The result once again indicates that small molecule design is a tricky process, and lots of factors should be considered collectively in balance.

CONCLUSION

In summary, two small molecule donor materials DRBDT-TT and DRBDT-STT, containing a central alkyl-TT-substituted BDT and alkylthio-TT-substituted BDT unit, respectively, were

designed and synthesized. The optimized devices based on DRBDT-TT and DRBDT-STT both exhibited PCEs over 8% with FFs over 0.70, which were ascribed to their ordered molecular packing, preferable morphologies with feature size around 20–30 nm, and well-balanced charge transport abilities. The slightly lower performance of DRBDT-STT with alkylthio side chain is believed due to its relatively poorer absorption. The structural reason behind this is that replacing the alkyl with alkylthio slightly decreased intermolecular interactions and led to a slightly larger $\pi-\pi$ stacking distance, which was attributed to the larger dihedral angle between the TT and BDT unit in molecule DRBDT-STT. These results indicate that a delicate and balanced molecular design, including the correlation between the molecule chemical structures and packing behavior, is still highly needed for achieving high performance of SM-OPVs.

EXPERIMENTAL SECTION

Materials. All reactions and manipulations were carried out under argon atmosphere with the use of standard Schlenk techniques. All starting materials were purchased from commercial suppliers and used without further purification unless indicated otherwise.

2-(2-Hexyldecyl)thieno[3,2-*b*]thiophene (Compound 2a). Under the protection of argon, *n*-butyllithium (2.0 M, 10 mL, 20.00 mmol)

was dropwise added to compound **1** (2.80 g, 20.00 mmol) in dry THF (20 mL) at -78°C over 0.5 h. After being stirred for 0.5 h, the mixture was warmed to room temperature and stirred for another 0.5 h. 7-(Bromomethyl)pentadecane (4.87 g, 16.00 mmol) then was added into the mixture at -78°C in one portion, and the mixture was warmed to room temperature and stirred for 12 h. Subsequently, the mixture was poured into water and extracted with petroleum ether (20 mL \times 2). The organic layer was washed with water and dried over anhydrous Na_2SO_4 for 3 h. After removal of solvent, the crude product was purified by silica gel using petroleum ether as eluent to afford compound **2a** as a colorless liquid (2.40 g, 41%). ^1H NMR (400 MHz, CDCl_3): δ 7.24 (d, 1H), 7.16 (d, 1H), 6.91 (s, 1H), 2.86 (d, 2H), 1.72–1.69 (m, 1H), 1.30–1.25 (m, 24H), 0.89–0.86 (m, 6H). ^{13}C NMR (100 MHz, CDCl_3): δ 147.29, 138.71, 137.59, 125.20, 119.46, 117.16, 40.00, 35.66, 33.22, 33.19, 31.95, 30.00, 29.68, 29.38, 26.62, 22.73, 14.16.

2-((2-Hexyldecyl)thio)thieno[3,2-b]thiophene (Compound 2b). Under the protection of argon, *n*-butyllithium (2.0 M, 10 mL, 20.00 mmol) was dropwise added to compound **1** (2.80 g, 20.00 mmol) in dry THF (40 mL) at -78°C over 1 h. After being stirred for 0.5 h, the mixture was warmed to room temperature and stirred for another 0.5 h. Sulfur powder (0.64 g, 20.00 mmol) then was added in one portion at 0°C . After being stirred for 2 h, 7-(bromomethyl)pentadecane (6.09 g, 20.00 mmol) was added into the mixture at 0°C . The mixture then was warmed to room temperature and stirred overnight. The reaction mixture was poured into ice water and extracted with petroleum ether (30 mL \times 2). The organic layer was washed with water and dried over anhydrous Na_2SO_4 for 3 h. After removal of solvent, the crude product was purified by silica gel using petroleum ether as eluent to afford compound **2b** as a colorless liquid (6.70 g, 85%). ^1H NMR (400 MHz, CDCl_3): δ 7.38 (d, 1H), 7.29 (s, 1H), 7.17 (d, 1H), 2.79 (d, 2H), 7.29 (s, 1H), 1.69–1.63 (m, 1H), 1.42–1.24 (m, 24H), 0.89–0.86 (m, 6H). ^{13}C NMR (100 MHz, CDCl_3): δ 141.49, 138.31, 138.13, 127.21, 125.31, 119.44, 44.43, 37.69, 32.82, 31.94, 31.87, 29.94, 29.62, 29.36, 26.43, 22.71, 14.16.

4,8-Bis(5-(2-hexyldecyl)thio)thieno[3,2-b]thiophen-2-yl)benzo[1,2-b:4,5-b']dithiophene (Compound 3a). Under the protection of argon, *n*-butyllithium (2.0 M, 3.60 mL, 7.20 mmol) was dropwise added to compound **2a** (2.40 g, 6.40 mmol) in dry THF (20 mL) at -78°C over 0.5 h. After being stirred for 0.5 h, the mixture was warmed to room temperature and stirred for another 0.5 h. Benzo[1,2-b:4,5-b']dithiophene-4,8-dione (0.56 g, 2.56 mmol) then was quickly added, and the reaction mixture was refluxed at 60°C for 2 h. The reaction mixture was cooled to room temperature, and a solution of $\text{SnCl}_2 \cdot 2\text{H}_2\text{O}$ (2.31 g, 10.24 mmol) in 10% HCl (20 mL) was added. The reaction mixture was stirred for another 2 h and then poured into ice water. The mixture was extracted with petroleum ether (20 mL \times 2). The organic layer was washed with water and dried over anhydrous Na_2SO_4 for 3 h. After removal of solvent, the crude product was purified by silica gel using petroleum ether as eluent to afford compound **3a** as a yellow liquid (1.40 g, 60%). ^1H NMR (400 MHz, CDCl_3): δ 7.66 (d, 2H), 7.53 (s, 2H), 7.42 (d, 2H), 6.98 (s, 2H), 2.85 (d, 4H), 1.72–1.67 (m, 2H), 1.35–1.28 (m, 48H), 0.89–0.85 (m, 12H). ^{13}C NMR (100 MHz, CDCl_3): δ 147.74, 139.48, 139.44, 139.37, 137.65, 136.82, 127.90, 124.31, 123.39, 120.45, 117.40, 40.11, 35.71, 33.27, 32.01, 31.67, 30.08, 29.75, 26.70, 22.78, 14.21. MS (MALDI-TOF) m/z : calcd for $\text{C}_{54}\text{H}_{74}\text{S}_6$ [M]⁺, 914.41; found, 914.43.

4,8-Bis(5-((2-hexyldecyl)thio)thieno[3,2-b]thiophen-2-yl)benzo[1,2-b:4,5-b']dithiophene (Compound 3b). Under the protection of argon, *n*-butyllithium (2.0 M, 6.6 mL, 13.20 mmol) was dropwise added to compound **2b** (4.76 g, 12.00 mmol) in dry THF (30 mL) at -78°C over 0.5 h. After being stirred for 0.5 h, the mixture was warmed to room temperature and stirred for another 0.5 h. Benzo[1,2-b:4,5-b']dithiophene-4,8-dione (0.88 g, 4.00 mmol) then was quickly added, and the reaction mixture was refluxed at 60°C for 2 h. The reaction mixture was cooled to room temperature, and a solution of $\text{SnCl}_2 \cdot 2\text{H}_2\text{O}$ (4.52 g, 20.00 mmol) in 10% HCl (30 mL) was added. The reaction mixture was stirred for another 2 h and then poured into ice water. The mixture was extracted with petroleum ether (20 mL \times 2). The organic layer was washed with water and dried over anhydrous

Na_2SO_4 for 3 h. After removal of solvent, the crude product was purified by silica gel using petroleum ether as eluent to afford compound **3b** as a yellow liquid (2.80 g, 71%). ^1H NMR (400 MHz, CDCl_3): δ 7.66 (d, 2H), 7.56 (s, 2H), 7.49 (d, 2H), 7.38 (s, 2H), 2.95 (d, 4H), 1.74–1.66 (m, 2H), 1.47–1.30 (m, 48H), 0.94–0.88 (m, 12H). ^{13}C NMR (100 MHz, CDCl_3): δ 141.39, 141.18, 139.41, 139.07, 138.92, 136.76, 128.19, 125.11, 124.06, 123.20, 120.38, 44.53, 37.78, 32.88, 31.97, 31.90, 30.00, 29.65, 29.40, 26.51, 22.75, 14.20. MS (MALDI-TOF) m/z : calcd for $\text{C}_{54}\text{H}_{74}\text{S}_8$ [M]⁺, 978.36; found, 978.24.

(4,8-Bis(5-(2-hexyldecyl)thieno[3,2-b]thiophen-2-yl)benzo[1,2-b:4,5-b']dithiophene-2,6-diyl)bis(tributylstannane) (Compound 4a). Under the protection of argon, *n*-butyllithium (2.0 M, 1.00 mL, 2.00 mmol) was dropwise added to compound **3a** (0.80 g, 0.90 mmol) in dry THF (20 mL) at -78°C over 0.5 h. After being stirred for 1 h, Bu_3SnCl (3.26 g, 10.00 mmol) was added into the mixture at -78°C over 0.5 h. The mixture then was warmed to room temperature and stirred for 12 h. Subsequently, the mixture was poured into ice water and extracted with CH_2Cl_2 (20 mL \times 2). The organic layer was washed with water and dried over anhydrous Na_2SO_4 for 3 h and concentrated to afford compound **4a**, which was used for the next step without purification.

(4,8-Bis(5-((2-hexyldecyl)thio)thieno[3,2-b]thiophen-2-yl)benzo[1,2-b:4,5-b']dithiophene-2,6-diyl)bis(tributylstannane) (Compound 4b). Under the protection of argon, *n*-butyllithium (2.0 M, 1.05 mL, 2.10 mmol) was dropwise added to compound **4a** (0.68 g, 0.70 mmol) in dry THF (20 mL) at -78°C over 0.5 h. After being stirred for 2 h, Bu_3SnCl (3.26 g, 10.00 mmol) was added into the mixture at -78°C over 0.5 h. The mixture was warmed to room temperature and stirred for 12 h. Subsequently, the mixture was poured into ice water and extracted with CH_2Cl_2 (20 mL \times 2). The organic layer was washed with water and dried over anhydrous Na_2SO_4 for 3 h and concentrated to afford compound **4b**, which was used for the next step without purification.

5,"5'"-(4,8-Bis(5-(2-hexyldecyl)thieno[3,2-b]thiophen-2-yl)benzo[1,2-b:4,5-b']dithiophene-2,6-diyl)bis(3,3"-diocetyl-[2,2'5':2"-terthiophene]-5-carbaldehyde) (Compound 6a). A solution of compound **4a** (0.90 mmol) and compound **5** (1.15 g, 1.98 mmol) in dry toluene (80 mL) was degassed twice with argon following the addition of $\text{Pd}(\text{PPh}_3)_4$ (0.12 g, 0.10 mmol). After being stirred and refluxed for 24 h at 110°C with the protection of argon, the reaction mixture was poured into water (100 mL) and extracted with CH_2Cl_2 (100 mL \times 2). The organic layer was washed with water twice and dried over anhydrous Na_2SO_4 for 3 h. After removal of solvent, the crude product was purified by silica gel using dichloromethane/petroleum (4:1) as eluent to afford compound **6a** as a red solid (1.10 g, 64%). ^1H NMR (400 MHz, CDCl_3): δ 9.82 (s, 2H), 7.67 (s, 2H), 7.59 (s, 2H), 7.58 (s, 2H), 7.23 (d, 2H), 7.12 (s, 2H), 7.11 (d, 2H), 7.05 (s, 2H), 2.92 (d, 4H), 2.83–2.79 (t, 4H), 2.76–2.72 (t, 4H), 1.75 (br, 2H), 1.72–1.63 (m, 8H), 1.39–1.26 (m, 90H), 0.92–0.85 (m, 24H). ^{13}C NMR (100 MHz, CDCl_3): δ 182.44, 148.03, 141.05, 140.97, 140.29, 140.18, 139.57, 139.07, 139.02, 138.92, 137.88, 137.72, 137.51, 135.38, 134.70, 130.52, 128.51, 127.77, 126.17, 123.43, 120.51, 118.88, 117.45, 40.10, 35.77, 33.23, 31.96, 31.91, 30.44, 30.27, 30.06, 29.72, 29.53, 29.44, 29.38, 29.30, 29.26, 26.65, 22.69, 14.17, 14.13. MS (MALDI-TOF) m/z : calcd for $\text{C}_{112}\text{H}_{150}\text{O}_2\text{S}_{12}$ [M]⁺, 1913.17; found, 1913.36.

5,"5'"-(4,8-Bis(5-((2-hexyldecyl)thio)thieno[3,2-b]thiophen-2-yl)benzo[1,2-b:4,5-b']dithiophene-2,6-diyl)bis(3,3"-diocetyl-[2,2'5':2"-terthiophene]-5-carbaldehyde) (Compound 6b). A solution of compound **4a** (0.70 mmol) and compound **5** (0.92 g, 1.54 mmol) in dry toluene (60 mL) was degassed twice with argon following the addition of $\text{Pd}(\text{PPh}_3)_4$ (0.08 g, 0.07 mmol). After being stirred and refluxed for 24 h at 110°C with the protection of argon, the reaction mixture was poured into water (100 mL) and extracted with CH_2Cl_2 (100 mL \times 2). The organic layer was washed with water twice and dried over anhydrous Na_2SO_4 for 3 h. After removal of solvent, the crude product was purified by silica gel using dichloromethane/petroleum (5:1) as eluent to afford compound **6b** as a red solid (0.60 g, 44%). ^1H NMR (400 MHz, CDCl_3): δ 9.84 (s, 2H), 7.63 (s, 2H), 7.60 (br, 4H), 7.41 (s, 2H), 7.24 (d, 2H), 7.13 (br, 4H), 3.01 (d, 4H),

2.85–2.81 (t, 4H), 2.76–2.73 (t, 4H), 1.75 (s, 2H), 1.88 (br, 2H), 1.72–1.67 (m, 8H), 1.41–1.32 (m, 90H), 0.92–0.87 (m, 24H). ^{13}C NMR (100 MHz, CDCl_3): δ 182.26, 141.22, 140.94, 140.57, 139.93, 139.81, 139.57, 139.08, 138.56, 137.79, 137.48, 137.02, 134.78, 134.55, 130.65, 128.31, 127.37, 125.73, 124.72, 122.74, 120.36, 118.27, 44.62, 37.94, 32.96, 31.98, 30.37, 30.14, 30.10, 29.91, 29.71, 29.57, 29.52, 29.44, 29.34, 26.57, 25.65, 22.77, 14.19. MS (MALDI-TOF) m/z : calcd for $\text{C}_{112}\text{H}_{150}\text{O}_2\text{S}_{14}$ [M] $^+$, 1974.77; found, 1974.87.

(5Z,5'Z)-5,5'-((5,5'-(5,5'-(4,8-Bis(5-(2-hexyldecyl)thiophen-2-yl)benzo[1,2-b:4,5-b']dithiophene-2,6-diyl)bis(3-octylthiophene-5,2-diyl))bis(thieno[3,2-b]thiophene-5,2-diyl))bis(4-octylthiophene-5,2-diyl))bis(methanlylidene))bis(3-ethyl-2-thioxothiazolidin-4-one) (DRBDT-TT). Compound **6a** (0.30 g, 0.16 mmol) and 3-ethylrhodanine (0.27 g, 1.60 mmol) were dissolved in a dry CHCl_3 (50 mL) solution under the protection of argon, and then three drops of piperidine were added to the mixture. After being stirred and refluxed for 12 h at 60 °C, the mixture was extracted with CHCl_3 (50 mL \times 2), and the organic layer was washed with water and dried over anhydrous Na_2SO_4 for 3 h. After removal of solvent, the crude product was purified by silica gel using chloroform as eluant. The crude product was recrystallized from CHCl_3 and hexane two times to afford DRBDT-TT as a black solid (0.27 g, 77%). ^1H NMR (400 MHz, CDCl_3): δ 7.71 (s, 2H), 7.61 (s, 2H), 7.58 (s, 2H), 7.17–7.15 (m, 4H), 7.04 (br, 6H), 4.19–4.14 (q, 4H), 2.94–2.92 (d, 4H), 2.79–2.85 (t, 4H), 2.72–2.70 (t, 4H), 1.78 (br, 2H), 1.70–1.62 (m, 8H), 1.40–1.27 (m, 80H), 0.92–0.87 (m, 30H). ^{13}C NMR (100 MHz, CDCl_3): δ 191.90, 167.16, 147.91, 140.72, 140.60, 139.63, 139.52, 139.09, 138.84, 137.71, 137.53, 137.29, 137.25, 135.08, 134.90, 134.57, 130.70, 128.37, 126.95, 125.84, 124.67, 123.17, 120.50, 120.34, 118.66, 117.52, 40.14, 39.87, 35.87, 33.27, 33.23, 32.00, 31.96, 31.91, 30.35, 30.10, 29.81, 29.74, 29.65, 29.53, 29.49, 29.37, 29.32, 26.69, 22.72, 14.14, 12.30. MS (MALDI-TOF) m/z : calcd for $\text{C}_{122}\text{H}_{160}\text{N}_2\text{O}_2\text{S}_{16}$ [M] $^+$, 2199.63; found, 2199.69. Anal. Calcd for $\text{C}_{122}\text{H}_{160}\text{N}_2\text{O}_2\text{S}_{16}$: C, 66.62; H, 7.33; N, 1.27. Found: C, 66.72; H, 7.52; N, 1.34.

(5Z,5'Z)-5,5'-((5,(5'-(4,8-Bis(5-(2-hexyldecyl)thio)thieno[3,2-b]-thiophen-2-yl)benzo[1,2-b:4,5-b']dithiophene-2,6-diyl)bis(3,3'-diocetyl-[2,2';5',2"-terthiophene]-5',5-diyl))bis(methanlylidene))bis(3-ethyl-2-thioxothiazolidin-4-one) (DRBDT-STT). Compound **6b** (0.32 g, 0.16 mmol) and 3-ethylrhodanine (0.27 g, 1.60 mmol) were dissolved in a dry CHCl_3 (50 mL) solution under the protection of argon, and then three drops of piperidine were added to the mixture. After being stirred and refluxed for 12 h at 60 °C, the mixture was extracted with CHCl_3 (50 mL \times 2), and the organic layer was washed with water and dried over anhydrous Na_2SO_4 for 3 h. After removal of solvent, the crude product was purified by silica gel using chloroform as eluant. The crude product was recrystallized from CHCl_3 and hexane two times to afford DRBDT-STT as a black solid (0.23 g, 66%). ^1H NMR (400 MHz, CDCl_3): δ 7.69 (s, 2H), 7.56 (br, 4H), 7.38 (s, 2H), 7.16–7.14 (m, 4H), 7.04–7.02 (br, 4H), 4.19–4.14 (q, 4H), 3.02–3.01 (d, 4H), 2.75 (br, 4H), 2.69 (br, 4H), 1.76 (m, 2H), 1.66–1.64 (m, 8H), 1.39–1.25 (m, 80H), 0.91–0.86 (m, 30H). ^{13}C NMR (100 MHz, CDCl_3): δ 190.09, 165.38, 139.48, 139.00, 138.90, 137.68, 137.33, 136.03, 135.60, 135.47, 135.38, 133.23, 132.95, 129.09, 126.70, 125.21, 124.20, 123.01, 122.84, 121.15, 118.69, 118.58, 116.61, 42.81, 38.07, 36.09, 31.12, 30.07, 28.55, 28.35, 28.20, 27.89, 27.65, 27.54, 24.68, 20.89, 12.31, 10.47. MS (MALDI-TOF) m/z : calcd for $\text{C}_{122}\text{H}_{160}\text{N}_2\text{O}_2\text{S}_{16}$ [M] $^+$, 2263.75; found, 2263.76. Anal. Calcd for $\text{C}_{122}\text{H}_{160}\text{N}_2\text{O}_2\text{S}_{16}$: C, 64.73; H, 7.12; N, 1.24. Found: C, 64.81; H, 7.02; N, 1.27.

Instruments and Characterization. The ^1H and ^{13}C NMR spectra were recorded on a Bruker AV400 spectrometer. Matrix assisted laser desorption/ionization time-of-flight mass spectrometry (MALDI-TOF) was performed on a Bruker Autoflex III LRF200-CID instrument. The thermogravimetric analysis (TGA) and differential scanning calorimetry (DSC) were carried out on a NETZSCH STA 409PC instrument under purified nitrogen gas flow. The heating rate for TGA and DSC testing is $10\text{ }^\circ\text{C min}^{-1}$, and the cooling rate for DSC is $10\text{ }^\circ\text{C min}^{-1}$. UV-vis spectra were obtained with a JASCO V-570 spectrophotometer.

Cyclic voltammetry (CV) experiments were performed with a LK98B II Microcomputer-based Electrochemical Analyzer. All CV measurements were carried out at room temperature with a conventional three-electrode configuration employing a glassy carbon electrode as the working electrode, a saturated calomel electrode (SCE) as the reference electrode, and a Pt wire as the counter electrode. Dichloromethane was distilled from calcium hydride under dry nitrogen immediately prior to use. Tetrabutylammonium phosphorus hexafluoride (Bu_4NPf_6 , 0.1 M) in dry dichloromethane was used as the supporting electrolyte, and the scan rate was 100 mV s^{-1} . The highest occupied molecular orbital (HOMO) and lowest unoccupied molecular orbital (LUMO) energy levels were calculated from the onset oxidation potential and the onset reduction potential, using the equation $E_{\text{HOMO}} = -(4.80 + E_{\text{onset}}^{\text{ox}})$, $E_{\text{LUMO}} = -(4.80 + E_{\text{onset}}^{\text{re}}$.

The geometry structures of DRBDT-TT and DRBDT-STT were optimized by using DFT calculations (B3LYP/6-31G*), and the frequency analysis was followed to ensure that the optimized structures were stable states. All calculations were carried out using Gaussian 09.⁶³

Atomic force microscopy (AFM) was performed using a Multimode 8 atomic force microscope in tapping mode. The transmission electron microscopy (TEM) investigation was performed on Philips Technical G² F20 at 200 kV. The specimen for TEM measurement was prepared by spin-casting the blend solution on ITO/PEDOT:PSS substrate, then floating the film on a water surface, and transferring to TEM grids. Grazing incidence wide-angle X-ray scattering (GIXD) and resonant soft X-ray scattering (RSoXS) were performed at beamline 7.3.3 and 11.0.1.2 at Lawrence Berkeley National Lab.

Space charge limited current (SCLC) mobility was measured using a diode configuration of ITO/PEDOT:PSS/donor:PC₇₁BM/Au for hole mobility and glass/Al/donor:PC₇₁BM/Al for electron mobility and fitting the results to a space charge limited form, where the SCLC equation is described by

$$J = \frac{9\epsilon_0\epsilon_r\mu_0 V^2}{8L^3} \exp\left(0.89\beta\sqrt{\frac{V}{L}}\right)$$

where J is the current density, L is the film thickness of the active layer, μ_0 is the mobility, ϵ_r is the relative dielectric constant of the transport medium, ϵ_0 is the permittivity of free space ($8.85 \times 10^{-12}\text{ F m}^{-1}$), and V ($=V_{\text{appl}} - V_{\text{bi}}$) is the internal voltage in the device, where V_{appl} is the applied voltage to the device and V_{bi} is the built-in voltage due to the relative work function difference of the two electrodes.

Solar Cell Fabrication and Testing. The devices were fabricated with a structure of glass/ITO/PEDOT:PSS/donor:PC₇₁BM/PFN-Br/Al. The ITO-coated glass substrates were cleaned by ultrasonic treatment in detergent, deionized water, acetone, and isopropyl alcohol under ultrasonication for 15 min each and subsequently dried by a nitrogen blow. A thin layer of PEDOT:PSS (Clevios P VP AI 4083, filtered at 0.45 μm) was spin-coated at 3000 rpm onto ITO surface. After being baked at $150\text{ }^\circ\text{C}$ for 20 min, the substrates were transferred into an argon-filled glovebox. Subsequently, the active layer was spin-coated from blend chloroform solutions with different ratios (weight-to-weight) of donor and PC₇₁BM. For the devices based on DRBDT-TT, the substrates were placed in a glass Petri dish containing 150 μL of chloroform for 90 s for solvent vapor annealing. For the devices based on DRBDT-STT, the substrates were placed in a glass Petri dish containing 150 μL of carbon disulfide for 120 s for solvent vapor annealing. The substrates then were removed. Finally, a thin layer of PFN-Br (5 nm) from its methanol solution was spin-coated, and 80 nm Al layer was deposited under high vacuum ($<2 \times 10^{-4}\text{ Pa}$). The effective areas of cells were 4 mm^2 defined by shadow masks. The current density–voltage ($J-V$) curves of photovoltaic devices were obtained by a Keithley 2400 source-measure unit. All masked and unmasked tests gave consistent results with relative errors within 5%. The photocurrent was measured under illumination simulated 100 mW cm^{-2} AM 1.5G irradiation using an Oriel 96000 solar simulator, calibrated with a standard Si solar cell. External quantum efficiencies

were measured using a Stanford Research Systems SR810 lock-in amplifier.

■ ASSOCIATED CONTENT

Supporting Information

The Supporting Information is available free of charge on the ACS Publications website at DOI: [10.1021/acs.chemmater.5b03889](https://doi.org/10.1021/acs.chemmater.5b03889).

Characterization data for the new compounds and additional experimental results ([PDF](#))

■ AUTHOR INFORMATION

Corresponding Authors

*E-mail: xjwan@nankai.edu.cn.

*E-mail: yschen99@nankai.edu.cn.

Author Contributions

[†]B.K. and Q.Z. contributed equally.

Notes

The authors declare no competing financial interest.

■ ACKNOWLEDGMENTS

We gratefully acknowledge financial support from MoST (2014CB643502), NSFC (51373078, 51422304, 91433101), PCSIRT (IRT1257), and Tianjin city (13RCGFGX01121). Portions of morphological characterization of the active layers were carried out at the Advanced Light Source, Berkeley National Laboratory, which was supported by the DOE-funded Energy Frontier Research Center on Polymer Based Materials for Harvesting Solar Energy (DE-SC0001087).

■ REFERENCES

- (1) Yu, G.; Gao, J.; Hummelen, J. C.; Wudl, F.; Heeger, A. J. Polymer Photovoltaic Cells: Enhanced Efficiencies via a Network of Internal Donor-Acceptor Heterojunctions. *Science* **1995**, *270*, 1789–1790.
- (2) Service, R. F. Outlook Brightens for Plastic Solar Cells. *Science* **2011**, *332*, 293–293.
- (3) Brabec, C. J.; Gowrisanker, S.; Halls, J. J.; Laird, D.; Jia, S.; Williams, S. P. Polymer-Fullerene Bulk-Heterojunction Solar Cells. *Adv. Mater.* **2010**, *22*, 3839–3856.
- (4) Li, G.; Zhu, R.; Yang, Y. Polymer Solar Cells. *Nat. Photonics* **2012**, *6*, 153–161.
- (5) Mei, J.; Bao, Z. Side Chain Engineering in Solution-Processable Conjugated Polymers. *Chem. Mater.* **2014**, *26*, 604–615.
- (6) Zhang, Z. G.; Li, Y. Side-Chain Engineering of High-Efficiency Conjugated Polymer Photovoltaic Materials. *Sci. China: Chem.* **2015**, *58*, 192–209.
- (7) Lu, L.; Zheng, T.; Wu, Q.; Schneider, A. M.; Zhao, D.; Yu, L. Recent Advances in Bulk Heterojunction Polymer Solar Cells. *Chem. Rev.* **2015**, *150807151721002*.
- (8) Lu, L.; Kelly, M. A.; You, W.; Yu, L. Status and Prospects for Ternary Organic Photovoltaics. *Nat. Photonics* **2015**, *9*, 491–500.
- (9) Liu, Y.; Chen, C. C.; Hong, Z.; Gao, J.; Yang, Y. M.; Zhou, H.; Dou, L.; Li, G.; Yang, Y. Solution-Processed Small-Molecule Solar Cells: Breaking the 10% Power Conversion Efficiency. *Sci. Rep.* **2013**, *3*, 3356.
- (10) Kan, B.; Zhang, Q.; Li, M.; Wan, X.; Ni, W.; Long, G.; Wang, Y.; Yang, X.; Feng, H.; Chen, Y. Solution-Processed Organic Solar Cells Based on Dialkylthiol-Substituted Benzodithiophene Unit with Efficiency Near 10%. *J. Am. Chem. Soc.* **2014**, *136*, 15529–15532.
- (11) Kan, B.; Li, M.; Zhang, Q.; Liu, F.; Wan, X.; Wang, Y.; Ni, W.; Long, G.; Yang, X.; Feng, H.; Zuo, Y.; Zhang, M.; Huang, F.; Cao, Y.; Russell, T. P.; Chen, Y. A Series of Simple Oligomer-like Small Molecules Based on Oligothiophenes for Solution-Processed Solar Cells with High Efficiency. *J. Am. Chem. Soc.* **2015**, *137*, 3886–3893.
- (12) Liao, S. H.; Jhuo, H. J.; Yeh, P. N.; Cheng, Y. S.; Li, Y. L.; Lee, Y. H.; Sharma, S.; Chen, S. A. Single Junction Inverted Polymer Solar Cell Reaching Power Conversion Efficiency 10.31% by Employing Dual-Doped Zinc Oxide Nano-Film as Cathode Interlayer. *Sci. Rep.* **2014**, *4*, 6813.
- (13) Liu, Y.; Zhao, J.; Li, Z.; Mu, C.; Ma, W.; Hu, H.; Jiang, K.; Lin, H.; Ade, H.; Yan, H. Aggregation and Morphology Control Enables Multiple Cases of High-Efficiency Polymer Solar Cells. *Nat. Commun.* **2014**, *5*, 5293.
- (14) Huang, J.; Li, C. Z.; Chueh, C. C.; Liu, S. Q.; Yu, J. S.; Jen, A. K. Y. 10.4% Power Conversion Efficiency of ITO-Free Organic Photovoltaics Through Enhanced Light Trapping Configuration. *Adv. Energy Mater.* **2015**, *5*, 1500406.
- (15) Jagadamma, L. K.; Al-Senani, M.; El-Labban, A.; Gereige, I.; Ngongang Ndjawa, G. O.; Faria, J. C. D.; Kim, T.; Zhao, K.; Cruciani, F.; Anjum, D. H.; McLachlan, M. A.; Beaujuge, P. M.; Amassian, A. Polymer Solar Cells with Efficiency > 10% Enabled via a Facile Solution-Processed Al-Doped ZnO Electron Transporting Layer. *Adv. Energy Mater.* **2015**, *5*, 1500204.
- (16) Chen, J. D.; Cui, C.; Li, Y. Q.; Zhou, L.; Ou, Q. D.; Li, C.; Li, Y.; Tang, J. X. Single-Junction Polymer Solar Cells Exceeding 10% Power Conversion Efficiency. *Adv. Mater.* **2015**, *27*, 1035–1041.
- (17) Ouyang, X.; Peng, R.; Ai, L.; Zhang, X.; Ge, Z. Efficient Polymer Solar Cells Employing a Non-Conjugated Small-Molecule Electrolyte. *Nat. Photonics* **2015**, *9*, 520–524.
- (18) Kim, J. Y.; Lee, K.; Coates, N. E.; Moses, D.; Nguyen, T. Q.; Dante, M.; Heeger, A. J. Efficient Tandem Polymer Solar Cells Fabricated by All-Solution Processing. *Science* **2007**, *317*, 222–225.
- (19) Duan, C.; Zhang, K.; Zhong, C.; Huang, F.; Cao, Y. Recent Advances in Water/Alcohol-Soluble π-Conjugated Materials: New Materials and Growing Applications in Solar Cells. *Chem. Soc. Rev.* **2013**, *42*, 9071–9104.
- (20) Chen, Y.; Wan, X.; Long, G. High Performance Photovoltaic Applications Using Solution-Processed Small Molecules. *Acc. Chem. Res.* **2013**, *46*, 2645–2655.
- (21) Kyaw, A. K.; Wang, D. H.; Wynands, D.; Zhang, J.; Nguyen, T. Q.; Bazan, G. C.; Heeger, A. J. Improved Light Harvesting and Improved Efficiency by Insertion of an Optical Spacer (ZnO) in Solution-Processed Small-Molecule Solar Cells. *Nano Lett.* **2013**, *13*, 3796–3801.
- (22) Coughlin, J. E.; Henson, Z. B.; Welch, G. C.; Bazan, G. C. Design and Synthesis of Molecular Donors for Solution-Processed High-Efficiency Organic Solar Cells. *Acc. Chem. Res.* **2014**, *47*, 257–270.
- (23) Gao, K.; Li, L.; Lai, T.; Xiao, L.; Huang, Y.; Huang, F.; Peng, J.; Cao, Y.; Liu, F.; Russell, T. P.; Janssen, R. A.; Peng, X. Deep Absorbing Porphyrin Small Molecule for High-Performance Organic Solar Cells with Very Low Energy Losses. *J. Am. Chem. Soc.* **2015**, *137*, 7282–7285.
- (24) Li, M.; Liu, F.; Wan, X.; Ni, W.; Kan, B.; Feng, H.; Zhang, Q.; Yang, X.; Wang, Y.; Zhang, Y.; Shen, Y.; Russell, T. P.; Chen, Y. Subtle Balance Between Length Scale of Phase Separation and Domain Purification in Small-Molecule Bulk-Heterojunction Blends under Solvent Vapor Treatment. *Adv. Mater.* **2015**, *27*, 6296.
- (25) Sun, K.; Xiao, Z.; Lu, S.; Zajaczkowski, W.; Pisula, W.; Hanssen, E.; White, J. M.; Williamson, R. M.; Subbiah, J.; Ouyang, J.; Holmes, A. B.; Wong, W. W.; Jones, D. J. A Molecular Nematic Liquid Crystalline Material for High-Performance Organic Photovoltaics. *Nat. Commun.* **2015**, *6*, 6013.
- (26) Zhang, Q.; Kan, B.; Liu, F.; Long, G.; Wan, X.; Chen, X.; Zuo, Y.; Ni, W.; Zhang, H.; Li, M.; Hu, Z.; Huang, F.; Cao, Y.; Liang, Z.; Zhang, M.; Russell, T. P.; Chen, Y. Small-Molecule Solar Cells with Efficiency Over 9%. *Nat. Photonics* **2014**, *9*, 35–41.
- (27) Mishra, A.; Bäuerle, P. Small Molecule Organic Semiconductors on the Move: Promises for Future Solar Energy Technology. *Angew. Chem., Int. Ed.* **2012**, *51*, 2020–2067.
- (28) Roncali, J.; Leriche, P.; Blanchard, P. Molecular Materials for Organic Photovoltaics: Small is Beautiful. *Adv. Mater.* **2014**, *26*, 3821–3838.

- (29) Yuan, L.; Zhao, Y.; Zhang, J.; Zhang, Y.; Zhu, L.; Lu, K.; Yan, W.; Wei, Z. Oligomeric Donor Material for High-Efficiency Organic Solar Cells: Breaking Down a Polymer. *Adv. Mater.* **2015**, *27*, 4229–4233.
- (30) Ni, W.; Li, M.; Liu, F.; Wan, X.; Feng, H.; Kan, B.; Zhang, Q.; Zhang, H.; Chen, Y. Dithienosilole Based Small Molecule Organic Solar Cells with an Efficiency Over 8%: Investigation of the Relationship Between the Molecular Structure and Photovoltaic Performance. *Chem. Mater.* **2015**, *27*, 6077–6084.
- (31) Beaujuge, P. M.; Fréchet, J. M. J. Molecular Design and Ordering Effects in π -Functional Materials for Transistor and Solar Cell Applications. *J. Am. Chem. Soc.* **2011**, *133*, 20009–20029.
- (32) Dou, L.; Liu, Y.; Hong, Z.; Li, G.; Yang, Y. Low-Bandgap Near-IR Conjugated Polymers/Molecules for Organic Electronics. *Chem. Rev.* **2015**, *150819103855004*.
- (33) Hwang, Y. J.; Courtright, B. A.; Ferreira, A. S.; Tolbert, S. H.; Jenekhe, S. A. 7.7% Efficient All-Polymer Solar Cells. *Adv. Mater.* **2015**, *27*, 4578–4584.
- (34) Jung, J. W.; Jo, J. W.; Chueh, C. C.; Liu, F.; Jo, W. H.; Russell, T. P.; Jen, A. K. Fluoro-Substituted n-Type Conjugated Polymers for Additive-Free All-Polymer Bulk Heterojunction Solar Cells with High Power Conversion Efficiency of 6.71%. *Adv. Mater.* **2015**, *27*, 3310–3317.
- (35) Lin, Y.; Wang, J.; Zhang, Z. G.; Bai, H.; Li, Y.; Zhu, D.; Zhan, X. An Electron Acceptor Challenging Fullerenes for Efficient Polymer Solar Cells. *Adv. Mater.* **2015**, *27*, 1170–1174.
- (36) Liu, C.; Yi, C.; Wang, K.; Yang, Y.; Bhatta, R. S.; Tsige, M.; Xiao, S.; Gong, X. Single-Junction Polymer Solar Cells with Over 10% Efficiency by a Novel Two-Dimensional Donor-Acceptor Conjugated Copolymer. *ACS Appl. Mater. Interfaces* **2015**, *7*, 4928–4935.
- (37) McAfee, S. M.; Topple, J. M.; Hill, I. G.; Welch, G. C. Key Components to the Recent Performance Increases of Solution Processed Non-Fullerene Small Molecule Acceptors. *J. Mater. Chem. A* **2015**, *3*, 16393–16408.
- (38) Vohra, V.; Kawashima, K.; Kakara, T.; Koganezawa, T.; Osaka, I.; Takimiya, K.; Murata, H. Efficient Inverted Polymer Solar Cells Employing Favourable Molecular Orientation. *Nat. Photonics* **2015**, *9*, 403–408.
- (39) Liang, Y.; Yu, L. A New Class of Semiconducting Polymers for Bulk Heterojunction Solar Cells with Exceptionally High Performance. *Acc. Chem. Res.* **2010**, *43*, 1227–1236.
- (40) Ni, W.; Li, M.; Wan, X.; Zuo, Y.; Kan, B.; Feng, H.; Zhang, Q.; Chen, Y. A New Oligobenzodithiophene End-Capped with 3-Ethyl-Rhodanine Groups for Organic Solar Cells with High Open-Circuit Voltage. *Sci. China: Chem.* **2015**, *58*, 339–346.
- (41) Ye, L.; Zhang, S.; Huo, L.; Zhang, M.; Hou, J. Molecular Design Toward Highly Efficient Photovoltaic Polymers Based on Two-Dimensional Conjugated Benzodithiophene. *Acc. Chem. Res.* **2014**, *47*, 1595–1603.
- (42) Li, M.; Ni, W.; Wan, X.; Zhang, Q.; Kan, B.; Chen, Y. Benzo[1,2-b:4,5-b']dithiophene (BDT)-based Small Molecules for Solution Processed Organic Solar Cells. *J. Mater. Chem. A* **2015**, *3*, 4765–4776.
- (43) McCulloch, I.; Heeney, M.; Bailey, C.; Genevicius, K.; Macdonald, I.; Shkunov, M.; Sparrowe, D.; Tierney, S.; Wagner, R.; Zhang, W.; Chabinyc, M. L.; Kline, R. J.; McGehee, M. D.; Toney, M. F. Liquid-Crystalline Semiconducting Polymers with High Charge-Carrier Mobility. *Nat. Mater.* **2006**, *5*, 328–333.
- (44) Cinar, M. E.; Ozturk, T. Thienothiophenes, Dithienothiophenes, and Thienoacenes: Syntheses, Oligomers, Polymers, and Properties. *Chem. Rev.* **2015**, *115*, 3036–3140.
- (45) Kim, J.-H.; Song, C. E.; Kim, B.; Kang, I. N.; Shin, W. S.; Hwang, D. H. Thieno[3,2-b]thiophene-Substituted Benzo[1,2-b:4,5-b']dithiophene as a Promising Building Block for Low Bandgap Semiconducting Polymers for High-Performance Single and Tandem Organic Photovoltaic Cells. *Chem. Mater.* **2014**, *26*, 1234–1242.
- (46) Li, Y.; Chang, C. Y.; Chen, Y.; Song, Y.; Li, C. Z.; Yip, H. L.; Jen, A. K. Y.; Li, C. The Effect of Thieno[3,2-b]thiophene on the Absorption, Charge Mobility and Photovoltaic Performance of Diketopyrrolopyrrole-Based Low Bandgap Conjugated Polymers. *J. Mater. Chem. C* **2013**, *1*, 7526–7533.
- (47) Huo, L.; Yi, Z.; Li, Y. Alkylthio-Substituted Polythiophene: Absorption and Photovoltaic Properties. *Macromol. Rapid Commun.* **2009**, *30*, 925–931.
- (48) Lee, D.; Hubijar, E.; Kalaw, G. J. D.; Ferraris, J. P. Enhanced and Tunable Open-Circuit Voltage Using Dialkylthio Benzo[1,2-b:4,5-b']dithiophene in Polymer Solar Cells. *Chem. Mater.* **2012**, *24*, 2534–2540.
- (49) Ye, L.; Zhang, S.; Zhao, W.; Yao, H.; Hou, J. Highly Efficient 2D-Conjugated Benzodithiophene-Based Photovoltaic Polymer with Linear Alkylthio Side Chain. *Chem. Mater.* **2014**, *26*, 3603–3605.
- (50) Cui, C.; Wong, W. Y.; Li, Y. Improvement of Open-Circuit Voltage and Photovoltaic Properties of 2D-Conjugated Polymers by Alkylthio Substitution. *Energy Environ. Sci.* **2014**, *7*, 2276–2284.
- (51) Kim, J. H.; Park, J. B.; Jung, I. H.; Yoon, S. C.; Kwak, J.; Hwang, D. H. New Alkylthio-thieno[3, 2-b]thiophene-Substituted Benzodithiophene-Based Highly Efficient Photovoltaic Polymer. *J. Mater. Chem. C* **2015**, *3*, 4250–4253.
- (52) Yang, T.; Wang, M.; Duan, C.; Hu, X.; Huang, L.; Peng, J.; Huang, F.; Gong, X. Inverted Polymer Solar Cells with 8.4% Efficiency by Conjugated Polyelectrolyte. *Energy Environ. Sci.* **2012**, *5*, 8208–8214.
- (53) Wessendorf, C. D.; Schulz, G. L.; Mishra, A.; Kar, P.; Ata, I.; Weideler, M.; Urdanilleta, M.; Hanisch, J.; Mena-Osteritz, E.; Lindén, M.; Ahlsweide, E.; Bäuerle, P. Efficiency Improvement of Solution-Processed Dithienopyrrole-Based A-D-A Oligothiophene Bulk-Heterojunction Solar Cells by Solvent Vapor Annealing. *Adv. Energy Mater.* **2014**, *14*, 1400266.
- (54) Wang, J. L.; Wu, Z.; Miao, J. S.; Liu, K. K.; Chang, Z. F.; Zhang, R. B.; Wu, H. B.; Cao, Y. Solution-Processed Diketopyrrolopyrrole-Containing Small-Molecule Organic Solar Cells with 7.0% Efficiency: In-Depth Investigation on the Effects of Structure Modification and Solvent Vapor Annealing. *Chem. Mater.* **2015**, *27*, 4338–4348.
- (55) Schulz, G.; Löbert, M.; Ata, I.; Urdanilleta, M.; Linden, M.; Mishra, A.; Bäuerle, P. Functional Tuning of A-D-A Oligothiophenes: The Effect of Solvent Vapor Annealing on Blend Morphology and Solar Cell Performance. *J. Mater. Chem. A* **2015**, *3*, 13738–13748.
- (56) Blom, P. W.; Mihailescu, V. D.; Koster, L. J. A.; Markov, D. E. Device Physics of Polymer: Fullerene Bulk Heterojunction Solar Cells. *Adv. Mater.* **2007**, *19*, 1551–1566.
- (57) Proctor, C. M.; Kuik, M.; Nguyen, T. Q. Charge Carrier Recombination in Organic Solar Cells. *Prog. Polym. Sci.* **2013**, *38*, 1941–1960.
- (58) He, C. Z.; Su, S. J.; Xu, M.; Wu, H. B.; Cao, Y. Enhanced Power-Conversion Efficiency in Polymer Solar Cells Using an Inverted Device Structure. *Nat. Photonics* **2012**, *6*, 591–595.
- (59) Guo, X.; Zhou, N.; Lou, S. J.; Smith, J.; Tice, D. B.; Hennek, J. W.; Ponce Ortiz, R.; Lopez Navarrete, J. T.; Li, S.; Strzalka, J.; Chen, L. X.; Chang, R. P. H.; Facchetti, A.; Marks, T. J. Polymer Solar Cells with Enhanced Fill Factors. *Nat. Photonics* **2013**, *7*, 825–833.
- (60) Liu, F.; Gu, Y.; Shen, X.; Ferdous, S.; Wang, H. W.; Russell, T. P. Characterization of the Morphology of Solution-Processed Bulk Heterojunction Organic Photovoltaics. *Prog. Polym. Sci.* **2013**, *38*, 1990–2052.
- (61) Rivnay, J.; Mannsfeld, S. C.; Miller, C. E.; Salleo, A.; Toney, M. F. Quantitative Determination of Organic Semiconductor Microstructure From the Molecular to Device Scale. *Chem. Rev.* **2012**, *112*, 5488–5519.
- (62) Smilgies, D. M. Scherrer Grain-Size Analysis Adapted to Grazing-Incidence Scattering with Area Detectors. *J. Appl. Crystallogr.* **2009**, *42*, 1030–1034.
- (63) Frisch, M.; Trucks, G.; Schlegel, H.; Scuseria, G.; Robb, M.; Cheeseman, J.; Scalmani, G.; Barone, V.; Mennucci, B.; Petersson, G. *Gaussian 09*, revision B.01; Gaussian, Inc.: Wallingford, CT, 2010.